Progress In Electromagnetics Research B, Vol. 98, 125–145, 2023

Diffraction by a Semi-Infinite Parallel-Plate Waveguide with Five-Layer Material Loading: Rigorous Wiener-Hopf Analysis

Kewen He* and Kazuya Kobayashi

Abstract—In this paper, the Wiener-Hopf technique is used to analyze the plane wave diffraction rigorously by a semi-infinite parallel-plate waveguide with five-layer material loading for E polarization. Introducing the Fourier transform of the unknown scattered field and applying boundary conditions in the transform domain, the problem is formulated in terms of the simultaneous Wiener-Hopf equations satisfied by unknown spectral functions. The Wiener-Hopf equations are solved exactly via the factorization and decomposition procedures leading to exact and approximate solutions. Taking the Fourier inverse of the solution in the transform domain, the scattered field in the real space is explicitly derived. For the region inside the waveguide, the scattered field is expressed in terms of the waveguide TE modes, whereas the field outside the waveguide is evaluated asymptotically with the aid of the saddle point method leading to a far field expression. Numerical examples of the radar cross section (RCS) are presented for various physical parameters and far field scattering characteristics of the waveguide are discussed in detail.

1. INTRODUCTION

Researchers in the field of electromagnetic theory are often faced with the prediction and reduction of the radar cross-section (RCS) of a target [1–5]. It is well known that the radar absorbing material and the shaping of targets are the main topics in the RCS study. The design and application of electromagnetic wave absorbers are very important for the research of electromagnetic wave scattering [6]. It is also important to note that a radar absorber composed of multiple media or multilayer radar absorbers has recently received much attention in predicting and reducing the RCS of objects [7, 8]. On the other hand, a complex object, such as an aircraft or a vehicle, can be modeled using simple geometric elements such as plates, shells, spheres, and edges. In the past, the scattering and diffraction properties of simple geometric elements have been analyzed to investigate how to predict or reduce the RCS of the object. One of the important geometries in this regard is an open-ended metallic waveguide cavity [1–6, 9]. This problem can be used as a typical model for duct structures such as aircraft jet engine intakes and fissures on the surfaces of more complicated bodies. A variety of efficient analysis methods such as high-frequency techniques, numerical methods, the hybrid ray-numerical approach, and the Kobayashi potential method have been developed and scattering problems involving cavities of various shapes have been analyzed [10–21]. The solutions obtained by these methods, however, may not be uniformly valid for arbitrary cavity dimensions.

The Wiener-Hopf technique is known as a powerful, rigorous approach in analyzing wave scattering and diffraction problems involving canonical geometries, since the edge condition, required for the uniqueness of the solutions for edged obstacles, is explicitly taken into account [22–28]. This fact results in a fast convergence of the Wiener-Hopf solutions over a broad frequency range from very low to extremely high frequencies. In the previous papers, we used the Wiener-Hopf technique to carry out a

Received 24 November 2022, Accepted 1 February 2023, Scheduled 16 February 2023
* Corresponding author: Kewen He (a18.58bh@g.chuo-u.ac.jp).
The authors are with the Department of Electrical, Electronic, and Communication Engineering, Chuo University, Japan.

rigorous RCS analysis of various two-dimensional cavities formed by a finite parallel-plate waveguide [29–34] and a semi-infinite parallel-plate waveguide [35–37]. Our final solutions have been verified to be valid over a broad frequency range and can be used to validate other commonly-used numerical methods and high-frequency ray techniques. In this paper, we will consider a semi-infinite parallel-plate waveguide with five-layer material loading and analyze the E-polarized plane wave diffraction by using the Wiener-Hopf technique. The solution procedure developed in this paper provides a significant extension of our prior work on the terminated, semi-infinite parallel plate waveguide with four-layer material loading [37]. It should be emphasized that the analysis for this generalized waveguide geometry becomes much more complicated than our previous paper since it is necessary to take into account the more complex, multiple reflection-refraction-diffraction effect occurring inside the waveguide.

By introducing the Fourier transform for the unknown scattered field and applying appropriate boundary conditions in the transform domain, the problem is formulated in terms of simultaneous Wiener-Hopf equations. The Wiener-Hopf equations are then solved in a formal sense using the factorization and decomposition procedure. It is important to note that the formal solutions contain infinite series terms with unknown coefficients. The edge condition will then be explicitly used to derive approximate expressions for the infinite series, resulting in highly accurate approximate solutions to the Wiener-Hopf equations. Our final solution is shown to be valid for arbitrary waveguide dimensions. Taking the inverse Fourier transform of the Wiener-Hopf solutions and evaluating the integral, we derive the TE mode expression for the scattered field inside the waveguide, whereas for the outside the waveguide, a far field expression is derived by using the saddle point method. We shall present representative numerical examples of the RCS for various physical parameters, and discuss the scattering characteristics of the waveguide in detail.

The time factor is assumed to be $e^{-i\omega t}$ and suppressed throughout this paper.

2. TRANSFORMED WAVE EQUATIONS

We consider the diffraction of an E-polarized plane wave by a semi-infinite parallel-plate waveguide with five-layer material loading as shown in Fig. 1, where the waveguide plates are infinitely thin, perfectly conducting, and uniform in the y-direction. The relative permittivity and permeability for (ε_m, μ_m), $m = 1, 2, 3, 4$, and 5 characterize the material layers I, II, III, IV, and V, respectively.

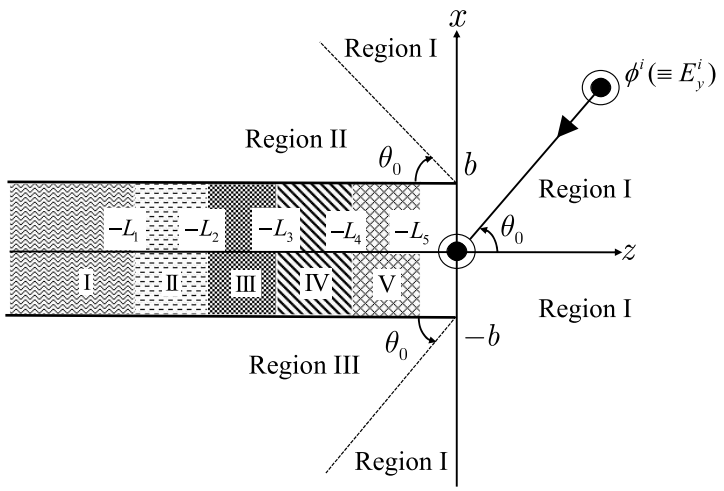

Figure 1. Geometry of the problem.

Let the total electric field $\phi^t(x, z)[\equiv E_y^t(x, z)]$ be

$$\phi^t(x, z) = \phi^i(x, z) + \phi(x, z) \tag{1}$$

for $-\infty < x < \infty$ and $-\infty < z < \infty$, where $\phi^i(x, z)$ is the incident field of E polarization defined by

$$\phi^i(x, z) = e^{-ik(x \sin\theta_0 + z \cos\theta_0)}, \quad 0 < \theta_0 < \pi/2 \tag{2}$$

with $k[\equiv \omega(\varepsilon_0\mu_0)^{1/2}]$ being the free-space wavenumber. The total field $\phi^t(x,z)$ satisfies the two-dimensional Helmholtz equation

$$[\partial^2/\partial x^2 + \partial^2/\partial z^2 + \varepsilon(x,z)\mu(x,z)k^2]\phi^t(x,z) = 0, \tag{3}$$

where

$$\mu(x,z) = \begin{cases} \mu_1\,(\text{layerI}) \\ \mu_2\,(\text{layerII}) \\ \mu_3\,(\text{layerIII}) \\ \mu_4\,(\text{layerIV}) \\ \mu_5\,(\text{layerV}) \\ 1\ (\text{otherwise}) \end{cases}, \qquad \varepsilon(x,z) = \begin{cases} \varepsilon_1\,(\text{layerI}) \\ \varepsilon_2\,(\text{layerII}) \\ \varepsilon_3\,(\text{layerIII}) \\ \varepsilon_4\,(\text{layerIV}) \\ \varepsilon_5\,(\text{layerV}) \\ 1\ (\text{otherwise}) \end{cases}, \tag{4}$$

Once the solution of (3) is found, nonzero components of the total electromagnetic fields are derived from

$$(E_y^t, H_x^t, H_z^t) = \left[\phi^t, \frac{i}{\omega\mu_0\mu\,(x,z)}\frac{\partial\phi^t}{\partial z}, \frac{1}{i\omega\mu_0\mu\,(x,z)}\frac{\partial\phi^t}{\partial x}\right]. \tag{5}$$

For the convenience of analysis, we shall assume that the vacuum is slightly lossy as in $k = k_1 + ik_2$ with $0 < k_2 \ll k_1$. The solution for the lossless case will be obtained by taking the limit $k_2 \to 0$ at the end of analysis. We now investigate the asymptotic behavior of the scattered field for $|z| \to \infty$. For convenience, let us define the cylindrical coordinates $(\rho_{1,2},\, \theta_{1,2})$ centered at the edges $(x,z) = (\pm b, 0)$ as

$$\left.\begin{array}{ll} x - b = \rho_1 \sin\theta_1, & z = \rho_1\cos\theta_1 \quad \text{for } 0 < \theta_1 < \pi, \\ x + b = \rho_2 \sin\theta_2, & z = \rho_2\cos\theta_2 \quad \text{for } -\pi < \theta_2 < 0, \end{array}\right\} \tag{6}$$

and introduce the following three regions:

$$\left.\begin{array}{l} \text{Region I} : \{(\rho_{1,2},\theta_{1,2}) : (0 < \rho_1 < \infty, -\pi/2 < \theta_1 < \pi - \theta_0) \\ \qquad \cup (0 < \rho_2 < \infty, -\pi + \theta_0 < \theta_1 < \pi/2)\} \\ \text{Region II} : \{(\rho_1,\theta_1) : (0 < \rho_1 < \infty, \pi - \theta_0 < \theta_1 < \pi)\} \\ \text{Region III} : \{(\rho_2,\theta_2) : (0 < \rho_2 < \infty, -\pi < \theta_2 < -\pi + \theta_0)\} \end{array}\right\} \tag{7}$$

Then we see from the radiation condition that the scattered field at large distances from the origin in Regions I, II, and III behaves like ϕ^d, $\phi^r + \phi^d$, and $-\phi^i + \phi^d$, respectively, where ϕ^r and ϕ^d denote the field reflected from the semi-infinite plate at $x = b$ and the diffracted field, respectively. Then by taking into account the fact that the semi-infinite parallel-plate waveguide can be regarded as a single semi-infinite plate in the far region, we can show that

$$\phi(x,z) = \begin{cases} O\left(e^{k_2 z\cos\theta_0}\right) & \text{as } z \to -\infty, \\ O\left(e^{-k_2 z}\right) & \text{as } z \to \infty. \end{cases} \tag{8}$$

for $-\infty < x < \infty$.

Let us define the Fourier transform of the scattered field with respect to z as

$$\Phi(x,\alpha) = (2\pi)^{-1/2}\int_{-\infty}^{\infty}\phi(x,z)e^{i\alpha z}dz, \tag{9}$$

where $\alpha = \sigma + i\tau(\equiv \text{Re}\alpha + i\text{Im}\alpha)$. In view of radiation condition, we can verify that $\Phi(x,\alpha)$ is regular in the strip $-k_2 < \tau < k_2\cos\theta_0$ of the complex α-plane. It is also proved that as $|x| \to \infty$, $\Phi(x,\alpha)$ is bounded for any α in $-k_2 < \tau < k_2\cos\theta_0$. Introducing the Fourier integrals as

$$\left.\begin{aligned} \Phi_+(x,\alpha) &= (2\pi)^{-1/2}\int_0^{\infty}\phi(x,z)e^{i\alpha z}dz, \\ \Phi_-(x,\alpha) &= (2\pi)^{-1/2}\int_{-\infty}^{-L_1}\phi^t(x,z)e^{i\alpha z}dz, \\ \Phi_m^r(x,\alpha) &= (2\pi)^{-1/2}\int_{-L_m}^{-L_{m+1}}\phi^t(x,z)e^{i\alpha z}dz,\ m = 1,2,3,4, \\ \Phi_1^0(x,\alpha) &= (2\pi)^{-1/2}\int_{-L_5}^{0}\phi^t(x,z)e^{i\alpha z}dz. \end{aligned}\right\} \tag{10}$$

we can show that $\Phi_+(x,\alpha)$ and $\Phi_-(x,\alpha)$ are regular in $\tau > -k_2$ and $\tau < k_2\cos\theta_0$, respectively, whereas $\Phi_1^0(x,\alpha)$ and $\Phi_m^r(x,\alpha)$ for $m = 1, 2, 3, 4$, are all entire functions. In the following analysis, we shall use these conventions for indicating the regions of regularity in the complex α-plane. Using (9) and (10), we can express $\Phi(x,\alpha)$ as

$$\Phi(x,\alpha) = \Phi_1(x,a) + \Psi_{(+)}(x,\alpha), \quad -\infty < x < \infty, \tag{11}$$

where

$$\Psi_{(+)}(x,\alpha) = \Phi_+(x,a) - A\frac{e^{-ikx\sin\theta_0}}{\alpha - k\cos\theta_0}, \quad A = \frac{1}{(2\pi)^{1/2}i}, \tag{12}$$

$$\Phi_1(x,\alpha) = \sum_{m=1}^{4}\Phi_m^r(x,\alpha) + \Phi_1^0(x,\alpha) + \Phi_-(x,\alpha). \tag{13}$$

As seen from (12), $\Psi_{(+)}(x,\alpha)$ is regular in the upper half-plane $\tau > -k_2$ except for a simple pole at $\alpha = k\cos\theta_0$. We shall henceforth use the subscript '(+)' for functions with this regularity property. In the following, we shall derive the transformed wave equations by taking into account the boundary conditions and the radiation condition.

In view of the boundary conditions for total tangential electromagnetic fields, we see that

$$E_y^t(\pm b, z) = 0, \quad -\infty < z < 0, \tag{14}$$

$$E_y^t(\pm b + 0, z) = E_y^t(\pm b - 0, z)\ [\equiv E_y^t(\pm b, z)], \quad 0 < z < \infty, \tag{15}$$

$$H_x^t(x, -L_m - 0) = H_x^t(x, -L_m + 0) \quad m = 1,2,3,4,5, \quad |x| < b. \tag{16}$$

Using (5), (14)–(16) can be rewritten as follows:

$$\phi^t(\pm b, z) = 0, \quad -\infty < z < 0, \tag{17}$$

$$\phi^t(\pm b + 0, z) = \phi^t(\pm b - 0, z)\ [\equiv \phi^t(\pm b, z)], \quad 0 < z < \infty, \tag{18}$$

$$\left.\begin{aligned} \frac{1}{\mu_m}\frac{\partial\phi^t(x,-L_m-0)}{\partial z} &= \frac{1}{\mu_{m+1}}\frac{\partial\phi^t(x,-L_m+0)}{\partial z}, \quad m = 1,2,3,4, \\ \frac{1}{\mu_5}\frac{\partial\phi^t(x,-L_5-0)}{\partial z} &= \frac{\partial\phi^t(x,-L_5+0)}{\partial z}. \end{aligned}\right\} \tag{19}$$

According to (1) and (3), the scattered field $\phi(x,z)$ in the vacuum region satisfies

$$(\partial^2/\partial x^2 + \partial^2/\partial z^2 + k^2)\phi(x,z) = 0. \tag{20}$$

In addition, the total field $\phi^t(x,z)$ satisfies

$$\left[\partial^2/\partial x^2 + \partial^2/\partial z^2 + \varepsilon(x,z)\mu(x,z)k_{rm}^2\right]\phi^t(x,z) = 0 \tag{21}$$

for $m = 1, 2, 3, 4$, and 5 for regions I, II, III, IV, and V, respectively, where $k_{rm} = (\mu_{rm}\varepsilon_{rm})^{1/2}k$. By taking the Fourier transform of (20) and applying (8) to the region $|x| > b$, we can verify that

$$\left(d^2/dx^2 - \gamma^2\right)\Phi(x,\alpha) = 0 \tag{22}$$

holds in the strip $-k_2 < \tau < k_2\cos\theta_0$, where

$$\gamma = \left(\alpha^2 - k^2\right)^{1/2}, \quad \mathrm{Re}\gamma > 0. \tag{23}$$

Since γ is a double-valued function of α, we choose $\mathrm{Re}\gamma > 0$ for its proper branch. Equation (22) is the transformed wave equation for $|x| > b$.

Because there are several medium discontinuities across the surfaces at $z = -L_m$ for $m = 1, 2, 3, 4$ and 5, the derivation of transformed wave equations for the region $|x| < b$ is complicated. We now multiply both sides of (20) by $(2\pi)^{-1/2}e^{i\alpha z}$ and integrate with respect to$z$ over the range $-L_5 < z < \infty$. Then by taking into account (8) and the boundary condition for tangential electromagnetic fields at $z = -L_5$, we derive that

$$(d^2/dx^2 - \gamma^2)\left[\Phi_1^0(x,\alpha) + \Psi_{(+)}(x,\alpha)\right] = e^{-i\alpha L_5}\left[\mu_{r5}^{-1}f_5(x) - i\alpha g_5(x)\right] \tag{24}$$

for $\tau > -k_2$ with $\alpha \neq k\cos\theta_0$, where

$$f_5(x) = (2\pi)^{-1/2}\frac{\partial\phi^t(x,-L_5-0)}{\partial z}, \tag{25}$$

$$g_5(x) = (2\pi)^{-1/2}\phi^t(x,-L_5-0). \tag{26}$$

Next, we multiply both sides of (21) by $(2\pi)^{-1/2}e^{i\alpha z}$ and integrate with respect to z over the ranges $-\infty < z < -L_1$, $-L_1 < z < -L_2$, $-L_2 < z < -L_3$, $-L_3 < z < -L_4$, and $-L_4 < z < -L_5$. Using the boundary conditions for tangential electromagnetic fields at $z = -L_m$ for $m = 1$, 2, 3, 4, and 5, we obtain

$$(d^2/dx^2 - \Gamma_1^2)\Phi_-(x,\alpha) = -e^{-i\alpha L_1}\left[f_1(x) - i\alpha g_1(x)\right], \tag{27}$$

$$\left(d^2/dx^2 - \Gamma_2^2\right)\Phi_1^r(x,\alpha) = -e^{-i\alpha L_2}\left[f_2(x) - i\alpha g_2(x)\right] + e^{-i\alpha L_1}\left[(\mu_{r2}/\mu_{r1})f_1(x) - i\alpha g_1(x)\right], \tag{28}$$

$$\left(d^2/dx^2 - \Gamma_3^2\right)\Phi_2^r(x,\alpha) = -e^{-i\alpha L_3}\left[f_3(x) - i\alpha g_3(x)\right] + e^{-i\alpha L_2}\left[(\mu_{r3}/\mu_{r2})f_2(x) - i\alpha g_2(x)\right], \tag{29}$$

$$\left(d^2/dx^2 - \Gamma_4^2\right)\Phi_3^r(x,\alpha) = -e^{-i\alpha L_4}\left[f_4(x) - i\alpha g_4(x)\right] + e^{-i\alpha L_3}\left[(\mu_{r4}/\mu_{r3})f_3(x) - i\alpha g_3(x)\right], \tag{30}$$

$$\left(d^2/dx^2 - \Gamma_5^2\right)\Phi_4^r(x,\alpha) = -e^{-i\alpha L_5}\left[f_5(x) - i\alpha g_5(x)\right] + e^{-i\alpha L_4}\left[(\mu_{r5}/\mu_{r4})f_4(x) - i\alpha g_4(x)\right] \tag{31}$$

where $\Gamma_m = (\alpha^2 - k_{rm}^2)^{1/2}$ with $\mathrm{Re}\Gamma_m > 0$ for $m = 1$, 2, 3, 4, 5, and

$$f_m(x) = (2\pi)^{-1/2}\frac{\partial\phi^t(x,-L_m-0)}{\partial z} \quad m = 1,2,3,4,5, \tag{32}$$

$$g_m(x) = (2\pi)^{-1/2}\phi^t(x,-L_m) \;\; m{=}\, 1,2,3,4,5. \tag{33}$$

Equations (24) and (27)–(31) are the transformed wave equations for $|x| < b$.

3. SCATTERED FIELD REPRESENTATION IN THE FOURIER TRANSFORM DOMAIN

Equations (8) and (9) show that $\Phi(x,\alpha)$ is bounded for $|x| \to \infty$, and therefore the solution of (22) is expressed as

$$\Phi(x,\alpha) = \begin{cases} \Psi_{(+)}(b,\alpha)e^{-\gamma(x-b)} & \text{for} \quad x > b, \\ \Psi_{(+)}(-b,\alpha)e^{\gamma(x+b)} & \text{for} \quad x < -b, \end{cases} \tag{34}$$

where we have used (11) and the following boundary conditions for tangential electric fields across $x = \pm b$:

$$\Phi_-(\pm b \pm 0,\alpha) = 0, \quad \Phi_1(\pm b \mp 0,\alpha) = 0, \tag{35}$$

$$\Phi_+(\pm b \pm 0,\alpha) = \Phi_+(\pm b - 0,\alpha)\left[\equiv \Phi_+(\pm b,\alpha)\right]. \tag{36}$$

Equation (34) is the scattered field representation for $|x| > b$.

Due to the medium discontinuities in $|x| < b$, the transformed wave equations contain unknown inhomogeneous terms $f_m(x)$ and $g_m(x)$ for $m = 1$, 2, 3, 4, 5 (see (24) and (27)–(31). In view of the edge condition, we can expand these functions into the Fourier sine series as

$$\left.\begin{matrix} f_m(x) \\ g_m(x) \end{matrix}\right\} = \frac{1}{b}\sum_{n=1}^{n}\left\{\begin{matrix} f_{mn} \\ g_{mn} \end{matrix}\right\}\sin\frac{n\pi}{2b}(x+b), \quad m = 1,2,3,4,5 \tag{37}$$

for $|x| < b$. Using (35) and (36) and carrying out some manipulations, we derive the solutions of (24) and (27)–(31) with the result that

$$\Phi_-(x,\alpha) = \frac{e^{-i\alpha L_1}}{b}\sum_{n=1}^{\infty}\frac{C_{1n}^-(\alpha)}{\alpha^2 + \Gamma_{1n}^2}\sin\frac{n\pi}{2b}(x+b), \tag{38}$$

$$\Phi_1^0(x,\alpha)+\Psi_{(+)}(x,\alpha) = \Psi_{(+)}(b,\alpha)\frac{\sinh\gamma(x+b)}{\sinh 2\gamma b}-\Psi_{(+)}(-b,\alpha)\frac{\sinh\gamma(x-b)}{\sinh 2\gamma b} -\frac{e^{-i\alpha L_5}}{b}\sum_{n=1}^{\infty}\frac{C_{5n}^{+}(\alpha)}{\alpha^2+\gamma_n^2}\sin\frac{n\pi}{2b}(x+b), \tag{39}$$

$$\Phi_m^r(x,\alpha) = \frac{1}{b}\sum_{n=1}^{\infty}\frac{C_{mn}(\alpha)}{\alpha^2+\Gamma_{mn}^2}\sin\frac{n\pi}{2b}(x+b), \quad m=1,2,3,4, \tag{40}$$

where

$$\gamma_n=\left[(n\pi/2b)^2-k^2\right]^{1/2}; \quad \Gamma_{mn}=\left[(n\pi/2b)^2-k_{rm}^2\right]^{1/2}, \quad m=1,2,3,4,5, \tag{41}$$

$$C_{5n}(\alpha)=e^{-i\alpha L_5}C_{5n}^{+}(\alpha), \tag{42}$$

$$C_{mn}(\alpha)=e^{-i\alpha L_{m+1}}C_{(m+1)n}^{-}(\alpha)-e^{-i\alpha L_m}C_{mn}^{+}(\alpha) \text{ for } m=1,2,3,4 \tag{43}$$

with

$$C_{mn}^{-}(\alpha)=f_{mn}-i\alpha g_{mn}, \quad m=1,2,3,4,5 \tag{44}$$

$$C_{mn}^{+}(\alpha)=(\mu_{rm+1}/\mu_{rm})f_{mn}-i\alpha g_{mn}, \quad m=2,3,4,5. \tag{45}$$

The scattered field representation for region $|x|<b$ is derived by substituting (24) and (27)–(31) into (13) and using (11).

We conclude from the above results that the desired scattered field representation in the Fourier transform domain leads to

$$\begin{aligned}\Phi(x,\alpha) &= \Psi_{(+)}(\pm b,\alpha)e^{\mp\gamma(x\mp b)} \text{ for } x\gtrless\pm b,\\ &= \Psi_{(+)}(b,\alpha)\frac{\sinh\gamma(x+b)}{\sinh 2\gamma b}-\Psi_{(+)}(-b,\alpha)\frac{\sinh\gamma(x-b)}{\sinh 2\gamma b}\\ &\quad -\frac{1}{b}\sum_{n=1}^{\infty}\frac{e^{-i\alpha L_5}C_{5n}^{+}(\alpha)}{\alpha^2+\gamma_n^2}\sin\frac{n\pi}{2b}(x+b)\\ &\quad -\frac{1}{b}\sum_{n=1}^{\infty}\frac{e^{-\alpha L_1}C_{1n}^{-}(\alpha)}{\alpha^2+\gamma_n^2}\sin\frac{n\pi}{2b}(x+b)\\ &\quad -\frac{1}{b}\sum_{m=1}^{4}\sum_{n=1}^{\infty}\frac{C_{mn}(\alpha)}{\alpha^2+\Gamma_{mn}^2}\sin\frac{n\pi}{2b}(x+b) \text{ for } |x|<b.\end{aligned} \tag{46}$$

Equation (46) holds in the strip $-k_2<\tau<k_2\cos\theta_0$ of the complex α-plane.

4. SIMULTANEOUS WIENER-HOPF EQUATIONS

Differentiating (46) with respect to x, setting $x=\pm b\pm 0$, $\pm b\mp 0$ in the results, and carrying out some manipulations with the aid of boundary conditions, we arrive at

$$\begin{aligned}J_{-}^{d}(\alpha) &= -\frac{U_{(+)}(\alpha)}{M(\alpha)}-\sum_{n=1,odd}^{\infty}\frac{n\pi}{b^2}\frac{e^{-i\alpha L_5}C_{5n}^{+}(\alpha)}{\alpha^2+\gamma_n^2}\\ &\quad +\sum_{n=1,odd}^{\infty}\frac{n\pi}{b^2}\frac{e^{-i\alpha L_1}C_{1n}^{-}(\alpha)}{\alpha^2+\Gamma_{1n}^2}\\ &\quad +\sum_{m=2}^{5}\sum_{n=1,odd}^{\infty}\frac{n\pi}{b^2}\frac{e^{-i\alpha L_m}C_{mn}^{-}(\alpha)-e^{-i\alpha L_{m-1}}C_{(m-1)n}^{+}(\alpha)}{\alpha^2+\Gamma_{mn}^2},\end{aligned} \tag{47}$$

$$J_-^s(\alpha) = -\frac{V_{(+)}(\alpha)}{N(\alpha)} + \sum_{n=2,even}^{\infty} \frac{n\pi}{b^2} \frac{e^{-i\alpha L_5} C_{5n}^+(\alpha)}{\alpha^2+\gamma_n^2} - \sum_{n=2,even}^{\infty} \frac{n\pi}{b^2} \frac{e^{-i\alpha L_1} C_{1n}^-(\alpha)}{\alpha^2+\Gamma_{1n}^2} - \sum_{m=2}^{5} \sum_{n=1,even}^{\infty} \frac{n\pi}{b^2} \frac{e^{-i\alpha L_m} C_{mn}^-(\alpha) - e^{-i\alpha L_{m-1}} C_{(m-1)n}^+(\alpha)}{\alpha^2+\Gamma_{mn}^2}, \quad (48)$$

where

$$U_{(+)}(\alpha) = \Psi_{(+)}(b,\alpha) + \Psi_{(+)}(-b,\alpha), \quad (49)$$

$$V_{(+)}(\alpha) = \Psi_{(+)}(b,\alpha) - \Psi_{(+)}(-b,\alpha), \quad (50)$$

$$J_-^d(\alpha) = J_-(b,\alpha) - J_-(-b,\alpha), \quad (51)$$

$$J_-^s(\alpha) = J_-(b,\alpha) + J_-(-b,\alpha), \quad (52)$$

$$M(\alpha) = \frac{e^{-\gamma b}\cosh\gamma b}{\gamma}, \quad N(\alpha) = \frac{e^{-\gamma b}\sinh\gamma b}{\gamma}, \quad (53)$$

$$J_-(\pm b,\alpha) = \Phi'_-(\pm b \pm 0,\alpha) - \Phi'_1(\pm b \mp 0,\alpha). \quad (54)$$

The prime in (54) denotes differentiation with respect to x. Equations (47) and (48) are the simultaneous Wiener-Hopf equations satisfied by unknown spectral functions.

5. ANALYTICAL PROPERTIES OF THE FOURIER COEFFICIENTS

In this section, we study analytical properties of the Fourier coefficients f_{mn} and g_{mn} for $m = 1, 2, 3, 4, 5$ that appear in (37). Based on the definition, $\Psi_{(+)}(x,\alpha)$ is regular in $\tau > -k_2$ except for a simple pole at $\alpha = k\cos\theta_0$, whereas $\Phi_-(x,\alpha)$ is regular in $\tau < k_2\cos\theta_0$. In addition, $\Phi_m^r(x,\alpha)$ with $m = 2, 3, 4, 5$, and $\Phi_1^0(x,\alpha)$ are all entire functions. Therefore, it follows that

$$\lim_{\alpha\to i\gamma_n} (\alpha - i\gamma_n)\left[\Phi_1^0(x,\alpha) + \Psi_{(+)}(x,\alpha)\right] = 0, \quad (55)$$

$$\lim_{\alpha\to -i\Gamma_{1n}} (\alpha + i\Gamma_{1n})\Phi_-(x,\alpha) = 0, \quad (56)$$

$$\lim_{\alpha\to \pm i\Gamma_{mn}} (\alpha \mp i\Gamma_{mn})\Phi_{m-1}^r(x,\alpha) = 0, \quad m = 2,3,4,5. \quad (57)$$

Substituting (38)–(40) into (55)–(57), we obtain that

$$C_{5n}^+(i\gamma_n) = \left(\frac{n\pi}{2b}\right) U_{(+)}(i\gamma_n) \quad \text{for odd } n,$$
$$= -\left(\frac{n\pi}{2b}\right) V_{(+)}(i\gamma_n) \quad \text{for even } n, \quad (58)$$

and

$$C_{mn}(\pm i\Gamma_{mn}) = 0, \quad n = 1,2,3,\ldots. \quad (59)$$

with $m = 2, 3, 4, 5$, where $U_{(+)}(\alpha)$ and $V_{(+)}(\alpha)$ are defined by (49) and (50). Equations (58) and (59) form a system of simultaneous algebraic equations that connects the functions $U_{(+)}(\alpha)$ and $V_{(+)}(\alpha)$ with the Fourier coefficients f_{nm} and g_{mn} for $m = 1, 2, 3, 4, 5$. By solving these equations for f_{nm} and g_{mn}, we derive that

$$f_{mn} = \frac{n\pi}{b} P_{mn} U_{(+)}(i\gamma_n) \quad \text{for odd } n,$$
$$= -\frac{n\pi}{b} P_{mn} V_{(+)}(i\gamma_n) \quad \text{for even } n. \quad (60)$$

$$g_{mn} = \frac{n\pi}{b} Q_{mn} U_{(+)}(i\gamma_n) \quad \text{for odd } n,$$
$$= -\frac{n\pi}{b} Q_{mn} V_{(+)}(i\gamma_n) \quad \text{for even } n. \quad (61)$$

where

$$P_{1n} = \frac{2\Gamma_{1n}e^{-\Gamma_{2n}(L_1-L_2)}}{(\mu_{r2}/\mu_{r1})\Gamma_{1n}+\Gamma_{2n}}\frac{(1+\delta_{1n})\Gamma_{2n}e^{-\Gamma_{3n}(L_2-L_3)}}{(\mu_{r3}/\mu_{r2})\Gamma_{2n}+\delta_{1n}\Gamma_{3n}} \cdot\frac{(1+\delta_{2n})\Gamma_{3n}e^{-\Gamma_{4n}(L_3-L_4)}}{(\mu_{r4}/\mu_{r3})\Gamma_{3n}+\delta_{2n}\Gamma_{4n}}\frac{(1-\delta_{4n})e^{-\Gamma_{5n}(L_4-L_5)}}{1-\rho_{4n}\delta_{4n}e^{-2\Gamma_{5n}(L_4-L_5)}}\frac{(1+\delta_{3n})\mu_{r5}\Gamma_{4n}}{(\mu_{r5}/\mu_{r4})\Gamma_{4n}+\delta_{3n}\Gamma_{5n}}, \quad (62)$$

$$P_{2n} = \frac{(1+\delta_{1n})\Gamma_{2n}e^{-\Gamma_{3n}(L_2-L_3)}}{(\mu_{r3}/\mu_{r2})\Gamma_{2n}+\delta_{1n}\Gamma_{3n}}\frac{(1+\delta_{2n})\Gamma_{3n}e^{-\Gamma_{4n}(L_3-L_4)}}{(\mu_{r4}/\mu_{r3})\Gamma_{3n}+\delta_{2n}\Gamma_{4n}} \cdot\frac{(1-\delta_{4n})e^{-\Gamma_{5n}(L_4-L_5)}}{1-\rho_{4n}\delta_{4n}e^{-2\Gamma_{5n}(L_4-L_5)}}\frac{(1+\delta_{3n})\mu_{r5}\Gamma_{4n}}{(\mu_{r5}/\mu_{r4})\Gamma_{4n}+\delta_{3n}\Gamma_{5n}}, \quad (63)$$

$$P_{3n} = \frac{(1+\delta_{2n})\Gamma_{3n}e^{-\Gamma_{4n}(L_3-L_4)}}{(\mu_{r4}/\mu_{r3})\Gamma_{3n}+\delta_{2n}\Gamma_{4n}}\frac{(1-\delta_{4n})e^{-\Gamma_{5n}(L_4-L_5)}}{1-\rho_{4n}\delta_{4n}e^{-2\Gamma_{5n}(L_4-L_5)}}\frac{(1+\delta_{3n})\mu_{r5}\Gamma_{4n}}{(\mu_{r5}/\mu_{r4})\Gamma_{4n}+\delta_{3n}\Gamma_{5n}}, \quad (64)$$

$$P_{4n} = \frac{(1-\delta_{4n})e^{-\Gamma_{5n}(L_4-L_5)}}{1-\rho_{4n}\delta_{4n}e^{-2\Gamma_{5n}(L_4-L_5)}}\frac{(1+\delta_{3n})\mu_{r5}\Gamma_{4n}}{(\mu_{r5}/\mu_{r4})\Gamma_{4n}+\delta_{3n}\Gamma_{5n}}, \quad (65)$$

$$P_{5n} = \frac{(1-\delta_{4n})e^{-\Gamma_{5n}(L_4-L_5)}}{1-\rho_{4n}\delta_{4n}e^{-2\Gamma_{5n}(L_4-L_5)}} \quad (66)$$

$$Q_{1n} = \rho_{1n}e^{-\Gamma_{2n}(L_1-L_2)}\frac{(1+\delta_{1n})\Gamma_{2n}e^{-\Gamma_{3n}(L_2-L_3)}}{(\mu_{r3}/\mu_{r2})\Gamma_{2n}+\delta_{1n}\Gamma_{3n}}\frac{(1+\delta_{2n})\Gamma_{3n}e^{-\Gamma_{4n}(L_3-L_4)}}{(\mu_{r4}/\mu_{r3})\Gamma_{3n}+\delta_{2n}\Gamma_{4n}} \cdot\frac{(1-\delta_{4n})e^{-\Gamma_{5n}(L_4-L_5)}}{1-\rho_{4n}\delta_{4n}e^{-2\Gamma_{5n}(L_4-L_5)}}\frac{(1+\delta_{3n})\mu_{r5}\Gamma_{4n}}{(\mu_{r5}/\mu_{r4})\Gamma_{4n}+\delta_{3n}\Gamma_{5n}}, \quad (67)$$

$$Q_{2n} = \rho_{2n}e^{-\Gamma_{3n}(L_2-L_3)}\frac{(1+\delta_{2n})\Gamma_{3n}e^{-\Gamma_{4n}(L_3-L_4)}}{(\mu_{r4}/\mu_{r3})\Gamma_{3n}+\delta_{2n}\Gamma_{4n}} \cdot\frac{(1-\delta_{4n})e^{-\Gamma_{5n}(L_4-L_5)}}{1-\rho_{4n}\delta_{4n}e^{-2\Gamma_{5n}(L_4-L_5)}}\frac{(1+\delta_{3n})\mu_{r5}\Gamma_{4n}}{(\mu_{r5}/\mu_{r4})\Gamma_{4n}+\delta_{3n}\Gamma_{5n}}, \quad (68)$$

$$Q_{3n} = \rho_{3n}e^{-\Gamma_{4n}(L_3-L_4)}\frac{(1-\delta_{4n})e^{-\Gamma_{5n}(L_4-L_5)}}{1-\rho_{4n}\delta_{4n}e^{-2\Gamma_{5n}(L_4-L_5)}}\frac{(1+\delta_{3n})\mu_{r5}\Gamma_{4n}}{(\mu_{r5}/\mu_{r4})\Gamma_{4n}+\delta_{3n}\Gamma_{5n}}, \quad (69)$$

$$Q_{4n} = \rho_{4n}\frac{(1-\delta_{4n})e^{-\Gamma_{5n}(L_4-L_5)}}{1-\rho_{4n}\delta_{4n}e^{-2\Gamma_{5n}(L_4-L_5)}}\mu_{r5}, \quad (70)$$

$$Q_{5n} = \frac{\rho_{4n}e^{-2\Gamma_{5n}(L_4-L_5)}-\delta_{4n}}{1-\rho_{4n}\delta_{4n}e^{-2\Gamma_{5n}(L_4-L_5)}} \quad (71)$$

with

$$\rho_{1n} = \frac{(\mu_{r2}/\mu_{r1})\Gamma_{1n}-\Gamma_{2n}}{(\mu_{r2}/\mu_{r1})\Gamma_{1n}+\Gamma_{2n}}, \quad (72)$$

$$\delta_{1n} = \frac{1-\rho_{1n}e^{-2\Gamma_{2n}(L_1-L_2)}}{1+\rho_{1n}e^{-2\Gamma_{2n}(L_1-L_2)}}, \quad (73)$$

$$\rho_{2n} = \frac{(\mu_{r3}/\mu_{r2})\Gamma_{2n}-\delta_{1n}\Gamma_{3n}}{(\mu_{r3}/\mu_{r2})\Gamma_{2n}+\delta_{1n}\Gamma_{3n}}, \quad (74)$$

$$\delta_{2n} = \frac{1-\rho_{2n}e^{-2\Gamma_{3n}(L_2-L_3)}}{1+\rho_{2n}e^{-2\Gamma_{3n}(L_2-L_3)}}, \quad (75)$$

$$\rho_{3n} = \frac{(\mu_{r4}/\mu_{r3})\Gamma_{3n}-\delta_{2n}\Gamma_{4n}}{(\mu_{r4}/\mu_{r3})\Gamma_{3n}+\delta_{2n}\Gamma_{4n}}. \quad (76)$$

$$\delta_{3n} = \frac{1-\rho_{3n}e^{-2\Gamma_{4n}(L_3-L_4)}}{1+\rho_{3n}e^{-2\Gamma_{4n}(L_3-L_4)}}, \quad (77)$$

$$\rho_{4n} = \frac{(\mu_{r5}/\mu_{r4})\Gamma_{4n} - \delta_{3n}\Gamma_{5n}}{(\mu_{r5}/\mu_{r4})\Gamma_{4n} + \delta_{3n}\Gamma_{5n}}, \tag{78}$$

$$\delta_{4n} = \frac{\mu_{r5}\gamma_n - \Gamma_{5n}}{\mu_{r5}\gamma_n + \Gamma_{5n}}. \tag{79}$$

By substituting (60) and (61) with $m = 5$ into (43) and setting $\alpha = -i\gamma_n$, we also obtain

$$\begin{aligned} C_{5n}(-i\gamma_n) &= \frac{n\pi}{2b} e^{-2\gamma_n L_5} Q_{5n} U_{(+)}(i\gamma_n) \quad \text{for odd } n, \\ &= -\frac{n\pi}{2b} e^{-2\gamma_n L_5} Q_{5n} V_{(+)}(i\gamma_n) \quad \text{for even } n, \end{aligned} \tag{80}$$

where

$$Q_5 = \frac{\rho_{4n} e^{-2\Gamma_{5n}(L_4 - L_5)} - \delta_{4n}}{1 - \rho_{4n}\delta_{4n} e^{-2\Gamma_{5n}(L_4 - L_5)}}. \tag{81}$$

The results derived in this section can be conveniently used in the next section to solve the Wiener-Hopf equations.

6. SOLUTIONS OF THE WIENER-HOPF EQUATIONS

The kernel functions $M(\alpha)$ and $N(\alpha)$ given by (53) are factorized as [24, 25]

$$\left.\begin{aligned} M(\alpha) = M_+(\alpha)M_-(\alpha) = M_+(\alpha)M_+(-\alpha), \\ N(\alpha) = N_+(\alpha)N_-(\alpha) = N_+(\alpha)N_+(-\alpha), \end{aligned}\right\} \tag{82}$$

where

$$\begin{aligned} M_+(\alpha) = {} & (\cos kb)^{1/2} e^{i\pi/4} (k+\alpha)^{-1/2} \exp\left(\frac{i\gamma b}{\pi} \ln \frac{\alpha - \gamma}{k}\right) \\ & \exp\left[\frac{i\alpha b}{\pi}\left(1 - C + \ln\frac{\pi}{2kb} + i\frac{\pi}{2}\right)\right] \prod_{n=1,odd}^{\infty} \left(1 + \frac{\alpha}{i\gamma_n}\right) e^{2i\alpha b/n\pi}, \end{aligned} \tag{83}$$

$$\begin{aligned} N_+(\alpha) = {} & \left(\frac{\sin kb}{k}\right)^{1/2} \exp\left(\frac{i\gamma b}{\pi} \ln \frac{\alpha - \gamma}{k}\right) \\ & \exp\left[\frac{i\alpha b}{\pi}\pi\left(1 - C + \ln\frac{\pi}{2kb} + i\frac{\pi}{2}\right)\right] \prod_{n=2,even}^{\infty} \left(1 + \frac{\alpha}{i\gamma_n}\right) e^{2i\alpha b/n\pi} \end{aligned} \tag{84}$$

with C ($= 0.57721566\ldots$) being Euler's constant.

According to (82)–(84), $M_\pm(\alpha)$ and $N_\pm(\alpha)$ are regular and nonzero in $\tau \gtrless \mp k_2$, and show the asymptotic behavior

$$M_\pm(\alpha), N_\pm(\alpha) \sim -(\mp i\alpha/2)^{1/2} \text{ as } \alpha \to \infty \text{ with } \tau \gtrless \mp k_2. \tag{85}$$

We multiply both sides of (47) by $M_-(\alpha)$ and decompose the resultant equations. This leads to

$$\begin{aligned} & M_-(\alpha)J_-^d(\alpha) - \left(\frac{2}{\pi}\right)^{1/2} \frac{i\cos(kb\sin\theta_0)}{M_+(k\cos\theta_0)(\alpha - k\cos\theta_0)} \\ & + \sum_{n=1,odd}^{\infty} \frac{n\pi}{b^2} \frac{1}{\alpha + i\gamma_n} \left[\frac{M_-(\alpha)e^{-i\alpha L_5} C_{5n}^+(\alpha)}{\alpha - i\gamma_n} + \frac{M_+(i\gamma_n)e^{-\gamma_n L_5} C_{5n}^+(-i\gamma_n)}{2i\gamma_n}\right] \\ & + \sum_{n=1,odd}^{\infty} \frac{n\pi}{b^2} \frac{1}{\alpha + i\gamma_n} \left[\frac{M_-(\alpha)e^{-i\alpha L_1} C_{1n}^-(\alpha)}{\alpha - i\Gamma_{1n}} + \frac{M_+(-i\Gamma_{1n})e^{-\Gamma_{1n} L_1} C_{1n}^+(-i\Gamma_{1n})}{2i\Gamma_{1n}}\right] \\ & + \sum_{m=2}^{5} \frac{1}{\alpha + i\Gamma_{mn}} \left\{ \frac{M_-(\alpha)\left[e^{-i\alpha L_m} C_{mn}^-(\alpha) - e^{-i\alpha L_{m-1}} C_{(m-1)n}^+(\alpha)\right]}{\alpha - i\Gamma_{mn}} \right. \end{aligned}$$

$$+\frac{M_+(i\Gamma_{mn})\left[e^{-i\alpha L_m}C^-_{mn}(-i\Gamma_{mn})-e^{-i\alpha L_{m-1}}C^+_{(m-1)n}(i\Gamma_{mn})\right]}{2i\Gamma_{mn}}\Bigg\}$$
$$=-\frac{U_{(+)}(\alpha)}{M_+(\alpha)}+\left(\frac{2}{\pi}\right)^{1/2}\frac{i\cos(kb\sin\theta_0)}{M_+(k\cos\theta_0)(\alpha-k\cos\theta_0)}$$
$$+\sum_{n=1,odd}^{\infty}\frac{n\pi}{b^2}\frac{M_+(i\gamma_n)e^{-\gamma_n L_5}C^+_{5n}(-i\gamma_n)}{2i\gamma_n(\alpha+i\gamma_n)}$$
$$-\sum_{n=1,odd}^{\infty}\frac{n\pi}{b^2}\frac{M_+(-i\Gamma_{1n})e^{-\Gamma_{1n}L_1}C^+_{1n}(-i\Gamma_{1n})}{2i\Gamma_{1n}(\alpha+i\Gamma_{1n})}$$
$$-\sum_{m=2,odd}^{5}\frac{n\pi}{b^2}\frac{M_+(-i\Gamma_{mn})\left[e^{-\Gamma_{mn}L_m}C^-_{mn}(-i\Gamma_{mn})-e^{-\Gamma_{mn}L_m}C^+_{mn}(-i\Gamma_{mn})\right]}{2i\Gamma_{mn}(\alpha+i\Gamma_{mn})}. \tag{86}$$

Based on Meixner's edge conditions [25, 38], we deduce that

$$\begin{aligned}&E_y^t=O(\rho^{1/2}),\ H^t=O(\rho^{-1/2}),\ \rho\to 0,\quad \text{for } L_5>0,\\ &E_y^t=O(\rho^{\nu}),\ H^t=O(\rho^{-1+\nu'}),\ \rho\to 0,\quad \text{for } L_5=0,\end{aligned} \tag{87}$$

$$\phi(\pm b,z)=\begin{cases}-e^{ik(\pm b\sin\theta_0)}+O(z^{1/2}),\ \text{for } L_5>0, \text{as } z\to+0,\\ -e^{ik(\pm b\sin\theta_0)}+O(z^{\nu}),\ \text{for } L_5=0, \text{as } z\to+0,\end{cases} \tag{88}$$

$$\frac{\partial\phi^t(\pm b\pm 0,z)}{\partial x}-\frac{\partial\phi^t(\pm b\mp 0,z)}{\partial x}=\begin{cases}O(z^{-1/2}), & \text{for } L_5>0, \text{as } z\to-0,\\ O(z^{-1+\nu'}), & \text{for } L_5=0,\ \text{as } z\to-0,\end{cases} \tag{89}$$

where ρ is the distance measured from the edges at the aperture of the waveguide, and

$$\nu=\eta(\nu_\mu,\nu_\varepsilon),\quad \nu'=\eta(\nu_\mu,\nu_\varepsilon+1) \tag{90}$$

with $\mathrm{Re}\nu>0$, $\mathrm{Re}\nu'>0$, and

$$\nu_\mu=\frac{1}{\pi}\cos^{-1}\frac{\mu_\gamma-1}{2(\mu_\gamma+1)},\quad \nu_\varepsilon=\frac{1}{\pi}\cos^{-1}\frac{1+\varepsilon_r}{2(1+\varepsilon_r)}, \tag{91}$$

$$\eta(a,b)=\begin{cases}a \text{ for } \mathrm{Re}a\le b,\\ b \text{ for } \mathrm{Re}a\le b.\end{cases} \tag{92}$$

Applying the fundamental theorem for the asymptotic behaviors of the Fourier integrals [26], we can show that $\Psi_{(+)}(\pm b,\alpha)$ and $J_-(\pm b,\alpha)$ asymptotically behave like

$$\begin{aligned}\Psi_{(+)}(\pm b,\alpha)=&O(\alpha^{-3/2}),\quad \text{for } \tau>-k_2,\quad \text{for } L_5>0,\\ =&O(\alpha^{-1-\nu}),\quad \text{for } \tau>-k_2,\quad \text{for } L_5=0,\end{aligned} \tag{93}$$

$$\begin{aligned}J_-(\pm b,\alpha)=&O(\alpha^{-1/2}),\quad \text{for } \tau<k_2\cos\theta_0,\quad \text{for } L_5>0,\\ =&O(\alpha^{-\nu'}),\quad \text{for } \tau<k_2\cos\theta_0,\quad \text{for } L_5=0.\end{aligned} \tag{94}$$

as $\alpha\to\infty$. Thus, applying (93) and (94) to (49), (50) and (51), (52) respectively, we can obtain

$$\begin{aligned}U_{(+)}(\alpha),V_{(+)}(\alpha)=&O(\alpha^{-3/2}),\quad \text{for } \tau>-k_2,\quad \text{for } L_5>0,\\ =&O(\alpha^{-1-\nu}),\quad \text{for } \tau>-k_2,\quad \text{for } L_5=0,\end{aligned} \tag{95}$$

$$\begin{aligned}J_-^{s,d}(\pm b,\alpha)=&O(\alpha^{-1/2}),\quad \text{for } \tau<k_2\cos\theta_0,\quad \text{for } L_5>0,\\ =&O(\alpha^{-\nu'}),\quad \text{for } \tau<k_2\cos\theta_0,\quad \text{for } L_5=0.\end{aligned} \tag{96}$$

It is shown that the left- and right-hand sides of (86) are regular in the lower ($\tau<k_2\cos\theta_0$) and upper ($\tau>-k_2$) half-planes, respectively, and both sides have a common strip of regularity

($-k_2 < \tau < k_2 \cos\theta_0$). As a result, the analytic continuation argument shows that both sides of (86) must be equal to an entire function, which is found to be identically zero by using (95), (96) and Liouville's theorem. It follows that

$$-\frac{U_{(+)}(\alpha)}{M_+(\alpha)} - \left(\frac{2}{\pi}\right)^{1/2} \frac{i\cos(kb\sin\theta_0)}{M_+(k\cos\theta_0)(\alpha - k\cos\theta_0)} + \sum_{n=1,odd}^{\infty} \frac{n\pi}{b^2} \frac{M_+(i\gamma_n)e^{-\gamma_n L_5} C_{5n}^+(-i\gamma_n)}{2i\gamma_n(\alpha + i\gamma_n)} = 0. \tag{97}$$

The Wiener-Hopf Equation (48) may be decomposed using a similar procedure. By multiplying both sides of (48) by $N_-(\alpha)$ and decomposing the resultant equation, we arrive at

$$-\frac{V_{(+)}(\alpha)}{N_+(\alpha)} + \left(\frac{2}{\pi}\right)^{1/2} \frac{\sin(kb\sin\theta_0)}{N_+(k\cos\theta_0)(\alpha - k\cos\theta_0)} - \sum_{n=2,even}^{\infty} \frac{n\pi}{b^2} \frac{N_+(i\gamma_n)e^{-\gamma_n L_5} C_{5n}^+(-i\gamma_n)}{2i\gamma_n(\alpha + i\gamma_n)} = 0. \tag{98}$$

The unknown coefficients $C_{5n}(-i\gamma_n)$ are involved in (97) and (98). In Section 5, we have examined the relationship between the unknown functions and the unknown Fourier coefficients. By substituting (80) into (97) and (98) and arranging the results, we obtain that

$$\frac{U_{(+)}(\alpha)}{b} = \frac{M_+(\alpha)}{b^{1/2}} \left[-\frac{A_u}{b\,(\alpha - k\cos\theta_0)} - \sum_{n=1}^{\infty} \frac{e^{-2\gamma_{2n-1}L_5} a_n p_n Q_{5n} u_n^+}{b\,(\alpha + i\gamma_{2n-1})} \right], \tag{99}$$

$$\frac{V_{(+)}(\alpha)}{b} = \frac{N_+(\alpha)}{b^{1/2}} \left[-\frac{A_v}{b\,(\alpha - k\cos\theta_0)} - \sum_{n=1}^{\infty} \frac{e^{-2\gamma_{2n}L_5} b_n q_n Q_{5n} v_n^+}{b\,(\alpha + i\gamma_{2n})} \right], \tag{100}$$

where

$$A_u = -\left(\frac{2}{\pi}\right)^{1/2} \frac{\cos(kb\sin\theta_0)}{M_+(k\cos\theta_0)}, \quad A_v = \left(\frac{2}{\pi}\right)^{1/2} \frac{\cos(kb\sin\theta_0)}{N_+(k\cos\theta_0)}, \tag{101}$$

$$a_n = \frac{[(n-1/2)\pi]^2}{bi\gamma_{2n-1}}, \quad b_n = \frac{(n\pi)^2}{bi\gamma_{2n}}, n \geq 1, \tag{102}$$

$$p_n = \frac{M_+(i\gamma_{2n-1})}{b^{1/2}}, \quad q_n = \frac{N_+(i\gamma_{2n})}{b^{1/2}}, n \geq 1, \tag{103}$$

$$u_n^+ = \frac{U_{(+)}(i\gamma_{2n-1})}{b}, \quad v_n^+ = \frac{V_{(+)}(i\gamma_{2n})}{b}, n \geq 1. \tag{104}$$

Equations (99) and (100) are the exact solutions to the Wiener-Hopf Equations (47) and (48). But they are formal since the infinite series with the unknown coefficients u_n^+ and v_n^+ for $n = 1, 2, 3, \ldots$ are involved. Therefore we need to develop a procedure to derive explicit approximate expressions of (99) and (100).

Using (95) and (104), it is possible to derive

$$\left.\begin{aligned} &u_n^+ \sim 2^{1/2} K_u (b\gamma_{2n-1})^{-3/2}, \quad v_n^+ \sim 2^{1/2} K_v (b\gamma_{2n})^{-3/2}, \quad \text{for } L_5 > 0, \\ &u_n^+ \sim 2^{1/2} K_u (b\gamma_{2n-1})^{-1-\nu}, \quad v_n^+ \sim 2^{1/2} K_v (b\gamma_{2n})^{-1-\nu}, \quad \text{for } L_5 = 0. \end{aligned}\right\} \tag{105}$$

as $n \to \infty$, where K_u and K_v are unknown constants. Taking a large positive integer N, the unknowns u_n^+ and v_n^+ for $n \geq N$ of the infinite series in (99) and (100) can be approximated with reasonable accuracy by the asymptotic behavior given in (105). We then replace each infinite series in (99) and (100) with the sum of a finite series containing $N-1$ unknowns and a remaining infinite series with one unknown constant. This procedure yields highly accurate approximate expression for the original infinite series since the edge condition is explicitly taken into account. Thus, we obtain the approximate expressions for (99) and (100) with the result that

$$\frac{U_{(+)}(\alpha)}{b} \approx \frac{M_+(\alpha)}{b^{1/2}} \left[-\frac{A_u}{b\,(\alpha - k\cos\theta_0)} - \sum_{n=1}^{N-1} \frac{e^{-2\gamma_{2n-1}L_5} a_n p_n Q_{5n} u_n^+}{b\,(\alpha + i\gamma_{2n-1})} + K_u S_u(\alpha) \right], \tag{106}$$

$$\frac{V_{(+)}(\alpha)}{b} \approx \frac{N_+(\alpha)}{b^{1/2}} \left[-\frac{A_v}{b\,(\alpha - k\cos\theta_0)} - \sum_{n=1}^{\infty} \frac{e^{-2\gamma_{2n}L_5} b_n q_n Q_{5n} v_n^+}{b\,(\alpha + i\gamma_{2n})} + K_v S_v(\alpha) \right], \tag{107}$$

where

$$\left.\begin{aligned} S_u^N(\alpha) &= \sum_{n=N}^{\infty} \frac{a_n Q_{5(2n-1)} e^{-2\gamma_{2n-1}L_5}(b\gamma_{2n-1})^{-2}}{b\,(\alpha + i\gamma_{2n-1})}, \\ S_v^N(\alpha) &= \sum_{n=N}^{\infty} \frac{b_n Q_{5(2n)} e^{-2\gamma_{2n}L_5}(b\gamma_{2n})^{-2}}{b\,(\alpha + i\gamma_{2n})}, \qquad \text{for } L_5 > 0, \\ S_u^N(\alpha) &= \sum_{n=N}^{\infty} \frac{a_n Q_{5(2n-1)} e^{-2\gamma_{2n-1}L_5}(b\gamma_{2n-1})^{-3/2-\nu}}{b\,(\alpha + i\gamma_{2n-1})}, \\ S_v^N(\alpha) &= \sum_{n=N}^{\infty} \frac{b_n Q_{5(2n)} e^{-2\gamma_{2n}L_5}(b\gamma_{2n})^{-3/2-\nu}}{b\,(\alpha + i\gamma_{2n})}, \quad \text{for } L_5 = 0. \end{aligned}\right\} \tag{108}$$

Equations (99) and (100) are approximate expressions of (47) and (48), respectively, where the unknowns u_n^+ and v_n^+ for $n = 1, 2, 3, \ldots, N-1, K_u$, and K_v are included. These unknowns can be efficiently determined by solving the two sets of $N \times N$ matrix equations numerically. It should be noted that (106) and (107) are uniformly valid for arbitrary aperture opening of the waveguide.

7. SCATTERED FIELD

The scattered field in real space can be obtained by taking the inverse Fourier transform according to the following formula:

$$\phi(x,z) = (2\pi)^{-1/2} \int_{-\infty+ic}^{\infty+ic} \Phi(x,\alpha) e^{-i\alpha z} d\alpha, \ -k_2 < c < k_2 \cos\theta_0. \tag{109}$$

Substituting (46) into (109), we can derive an integral representation for the scattered field valid for the entire space. In the following, we will analytically derive explicit expressions for the fields inside and outside the waveguide. The scattered field inside the waveguide can be expressed in terms of the TE modes by evaluating (109) using the residue theorem. For the region outside the waveguide, an asymptotic expression will be derived using the saddle point method.

First we consider the field inside the waveguide. Substituting the scattered field expression for $|x| < b$ in (46) into (109) and evaluating the resultant integral for $z < 0$ with the aid of (99) and (100), the scattered field inside the waveguide is shown to take form of

$$\begin{aligned} \phi(x,z) &= -\phi^i(x,z) + \sum_{n=1}^{\infty} T_{1n}^- e^{\Gamma_{1n}(z+L_1)} \sin\frac{n\pi}{2b}(x+b) \quad \text{for } -\infty < z < -L_1, \text{ (region I)}, \\ &= -\phi^i(x,z) + \sum_{n=1}^{\infty} \left[T_{mn}^- e^{\Gamma_{mn}(z+L_m)} - T_{mn}^+ e^{\Gamma_{mn}(z+L_{(m-1)})} \right] \sin\frac{n\pi}{2b}(x+b), \\ &\quad (m = 2,3,4,5) \text{for} - L_1 < z < -L_5, \text{ (region II, III, IV, V)} \\ &= -\phi^i(x,z) + \sum_{n=1}^{\infty} \left[T_0^- e^{\gamma_n(z+L_5)} - T_0^+ e^{-\gamma_n(z+L_5)} \right] \sin\frac{n\pi}{2b}(x+b), \text{ for} - L_5 < z < 0, \text{ (otherwise)}, \end{aligned} \tag{110}$$

where

$$\begin{aligned} T_{mn}^- &= \left(\frac{\pi}{2}\right)^{1/2} \frac{n\pi}{2b^2} \frac{P_{mn}}{\Gamma_{mn}} e^{-\gamma_n L_5} U_{(+)}(i\gamma_n), \quad \text{for odd } n, \quad (m = 1,2,3,4,5), \\ &= -\left(\frac{\pi}{2}\right)^{1/2} \frac{n\pi}{2b^2} \frac{P_{mn}}{\Gamma_{mn}} e^{-\gamma_n L_5} V_{(+)}(i\gamma_n), \quad \text{for even } n, \quad (m = 1,2,3,4,5). \end{aligned} \tag{111}$$

$$T_{mn}^{+} = \left(\frac{\pi}{2}\right)^{1/2} \frac{n\pi}{2b^2} \frac{Q_{mn}}{\Gamma_{(m+1)n}} e^{-\gamma_n L_5} U_{(+)}(i\gamma_n), \quad \text{for odd } n, \quad (m = 1, 2, 3, 4),$$
$$= -\left(\frac{\pi}{2}\right)^{1/2} \frac{n\pi}{2b^2} \frac{Q_{mn}}{\Gamma_{(m+1)n}} e^{-\gamma_n L_5} V_{(+)}(i\gamma_n), \quad \text{for even } n, \quad (m = 1, 2, 3, 4). \tag{112}$$

$$T_{0}^{-} = \left(\frac{\pi}{2}\right)^{1/2} \frac{n\pi}{2b^2} \frac{e^{-\gamma_n L_5}}{\gamma_n} U_{(+)}(i\gamma_n), \quad \text{for odd } n,$$
$$= -\left(\frac{\pi}{2}\right)^{1/2} \frac{n\pi}{2b^2} \frac{e^{-\gamma_n L_5}}{\gamma_n} V_{(+)}(i\gamma_n), \quad \text{for even } \ n. \tag{113}$$

$$T_{0}^{+} = \left(\frac{\pi}{2}\right)^{1/2} \frac{n\pi}{2b^2} \frac{Q_{5n}}{\gamma_n} e^{-\gamma_n L_5} U_{(+)}(i\gamma_n), \quad \text{for odd } n,$$
$$= -\left(\frac{\pi}{2}\right)^{1/2} \frac{n\pi}{2b^2} \frac{Q_{5n}}{\gamma_n} e^{-\gamma_n L_5} V_{(+)}(i\gamma_n), \quad \text{for even } n. \tag{114}$$

In (110)–(114), P_{mn} and Q_{mn} for $m = 1$, 2, 3, 4, 5 are defined in Section 5.

Next, we examine the field outside the waveguide and derive the scattered far field. The region outside the waveguide consists of region $|x| < b$ with $z > 0$ and region $|x| > b$. However, at large distances from the origin, contributions from $|x| < b$ outside the waveguide is negligibly small. Using (46) and (109), an integral representation of the scattered field is found to be

$$\phi(x, z) = (2\pi)^{-1/2} \int_{-\infty+ic}^{\infty+ic} \Psi_{(+)}\left(\pm b, \alpha\right) e^{\mp\gamma(x\mp b) - i\alpha z} d\alpha, \tag{115}$$

where $\Psi_{(+)}\left(\pm b, \alpha\right)$ can be expressed as follows (see (49) and (50)):

$$\Psi_{(+)}(\pm b, \alpha) = \frac{1}{2}\left[U_{(+)}(\alpha) \pm V_{(+)}(\alpha)\right]. \tag{116}$$

Applying the method developed in [37] and carrying out some manipulations, we are led to

$$\begin{aligned}\phi(\rho_{1,2}, \theta_{1,2}) \ \sim \ & \left[\Psi_{(+)}\left(\pm b, -k\cos\theta_{1,2}\right) - \tilde{\Phi}\left(\pm b, -k\cos\theta_{1,2}\right)\right] k\sin\theta_{1,2} \frac{e^{i(k\rho_{1,2} - \pi/4)}}{\left(k\rho_{1,2}\right)^{1/2}} \\ & - e^{\mp ikb\sin\theta_0} \left(e^{-ik\rho_{1,2}\cos(\theta_{1,2} - \theta_0)} F\left\{\left(2k\rho_{1,2}\right)^{1/2} \cos\left[\left(\theta_{1,2} - \theta_0\right)/2\right]\right\}\right. \\ & \left. + e^{-ik\rho_{1,2}\cos(\theta_{1,2} + \theta_0)} F\left\{\left(2k\rho_{1,2}\right)^{1/2} \cos\left[\left(\theta_{1,2} + \theta_0\right)/2\right]\right\}\right), x \gtrless \pm b. \end{aligned} \tag{117}$$

where $(\rho_{1,2}, \theta_{1,2})$ are the cylindrical coordinates given by (6), and $F\left(\cdot\right)$ is the Fresnel integral defined by

$$F\left(\omega\right) = \frac{e^{-i\pi/4}}{\pi^{1/2}} \int_{\omega}^{\infty} e^{it^2} dt. \tag{118}$$

Equation (117) provides an asymptotic expression of the scattered field as $k\rho_{1,2} \to \infty$, which is uniformly valid in observation angles $\theta_{1,2}$.

Introducing the cylindrical coordinate (ρ, θ) as $x = \rho\sin\theta$, $z = \rho\cos\theta$ for $-\pi < \theta < \pi$, it can be seen that the following approximate relationship holds in the far field.

$$\cos\theta_1 \approx \cos\theta \approx \cos\theta_2, \tag{119}$$

$$\rho_1 \approx \rho - b\sin\theta, \quad \text{for } 0 < \theta < \pi, \tag{120}$$

$$\rho_2 \approx \rho + b\sin\theta, \quad \text{for } -\pi < \theta < 0. \tag{121}$$

Replacing the Fresnel integral in (117) with its asymptotic expansion for large $|k|\,\rho_{1,2}$ and using (119)–(121), we can derive an alternative expression for the scattered far field

$$\phi\left(\rho, \theta\right) \sim \phi^g\left(\rho, \theta\right) + \phi^d\left(\rho, \theta\right), \quad \theta_{1,2} \not\approx \pi \mp \theta_0. \tag{122}$$

where $\phi^g(\rho,\theta)$ and $\phi^d(\rho,\theta)$ are the geometrical optics field and the diffraction field, respectively, and are defined by

$$\phi^g(\rho,\theta) = \begin{cases} -e^{-ik\rho\cos(\theta-\theta_0)}, & \text{for } -\pi < \theta_2 < \pi+\theta_0, \\ 0, & \text{for } -\pi+\theta_0 < \theta_2 < 0, 0 < \theta_1 < \pi-\theta_0, \\ -e^{-2ikb\sin\theta_0}e^{-ik\rho\cos(\theta+\theta_0)}, & \text{for } \pi-\theta_0 < \theta_1 < \pi. \end{cases} \tag{123}$$

$$\phi^d(\rho,\theta) = \Psi_{(+)}(\pm b, -k\cos\theta)\, k\sin\theta e^{\mp ikb\sin\theta}\frac{e^{i(k\rho-\pi/4)}}{(k\rho)^{1/2}}, \quad \text{for } \theta \gtrless 0. \tag{124}$$

8. NUMERICAL RESULTS AND DISCUSSION

In this section, we will show illustrative numerical examples of the RCS to investigate the far field backscattering characteristics of the waveguide in detail. The RCS per unit length is defined by

$$\sigma = \lim_{\rho\to\infty}\left(2\pi\rho\frac{\left|\phi^d\right|^2}{\left|\phi^i\right|^2}\right), \tag{125}$$

where ϕ^d is the diffracted field defined by (124). For real k, (125) is simplified by using (2), (116), and (124) as

$$\sigma = \lambda\left|\frac{k\sin\theta}{2}U_{(+)}(-k\cos\theta) \pm V_{(+)}(-k\cos\theta)\right|^2 \tag{126}$$

for $\theta \gtrless 0$ with λ being the free-space wavelength. We used the approximate expressions (106) and (107) to calculate $U_{(+)}(-k\cos\theta)$ and $V_{(+)}(-k\cos\theta)$ involved in (126). Since (106) and (107) contain the unknowns u_n^+, v_n^+ for $n = 1, 2, 3, \ldots, N-1$ and $K_{u,v}$, we need to invert the two sets of $N\times N$ matrix equations numerically for obtaining physical quantities. We have verified through careful investigation that choosing $N \geq 2kb/\pi$ in (106) and (107) gives sufficiently accurate results.

Figures 2–5 show the normalized monostatic RCS σ/λversus the incidence angle θ_0, where the value of σ/λ is plotted in decibels [dB] by calculating $10\log_{10}(\sigma/\lambda)$. To study the scattering mechanism over a broad frequency range, we have performed numerical calculations for six typical values of the normalized waveguide aperture width $kb = 1.57$, 3.14, 15.7, 31.4, 47.1, 62.8. Here $kb = 1.57$, 3.14 correspond to low frequencies, $kb = 15.7$, 31.4 correspond to medium frequencies, and $kb = 47.1$, 62.8 correspond to high frequencies. In addition, the ratio $L_1/2b$ has been chosen as 0.5 (Fig. 2), 1.0 (Fig. 3), 3.0 (Fig. 4), and 5.0 (Fig. 5). In numerical computations, we have used five different materials from the study of radar absorbing materials (RAM) by Michielssen et al. [6]. Although these material properties are fictitious, they represent a wide range of available radar absorbing materials. The material constants of the five-layer material inside the waveguide (see Fig. 1) are $\varepsilon_1 = 8+i10$, $\mu_1 = 1+i0$ for region I $\varepsilon_2 = 10+i6$, $\mu_2 = 1+i0$ for region II $\varepsilon_3 = 15+i0$, $\mu_3 = 3+i15$ for region III $\varepsilon_4 = 15+i0$, $\mu_4 = 7+i12$ for region IV, and $\varepsilon_5 = 15+i0$, $\mu_5 = 25.8+i10.3$ for region V. Here the material in region I extends from $z = -L_1$ to $-\infty$. The thickness of regions II, III, IV, and V is such that $L_1 - L_2 = L_2 - L_3 = L_3 - L_4 = L_4 - L_5 (= t/4)$ with t being the total thickness of the four-layer materials (regions II-V), which is taken as $kt = 1.57$. The results for the four cases of single, two-, three-, and four-layer material loading have been included in Figs. 2–5 for detailed comparisons.

General features observed from Figs. 2–5 are that, at medium ($kb = 15.7$, 31.4) and high ($kb = 47.1$, 62.8) frequencies, the RCS is reduced with an increase of the number of material layers. At low frequencies ($kb = 1.57$, 3.14), however, the RCS characteristics are very different from those at mid- and high-frequencies. This is because, the effect of diffracted waves generated at low frequencies is more significant than higher frequencies. At low frequencies, the scattered field shows complicated features and geometrical optics interpretation cannot be applied. From Figs. 2((a), (b)), 3((a), (b)), 4((a), (b)), 5((a), (b)), it is clear that the RCS value does not necessarily decrease with an increase of the number of layers. In particular, the RCS curves for the five different cases (single-, two-, three-, four, five-layer loading) in Figs. 4(a) and 5(a) merge and show 'single-line' like characteristics. This is noticeable in Fig. 5(a) and can be expected since in this case, the waveguide aperture opening is very small and

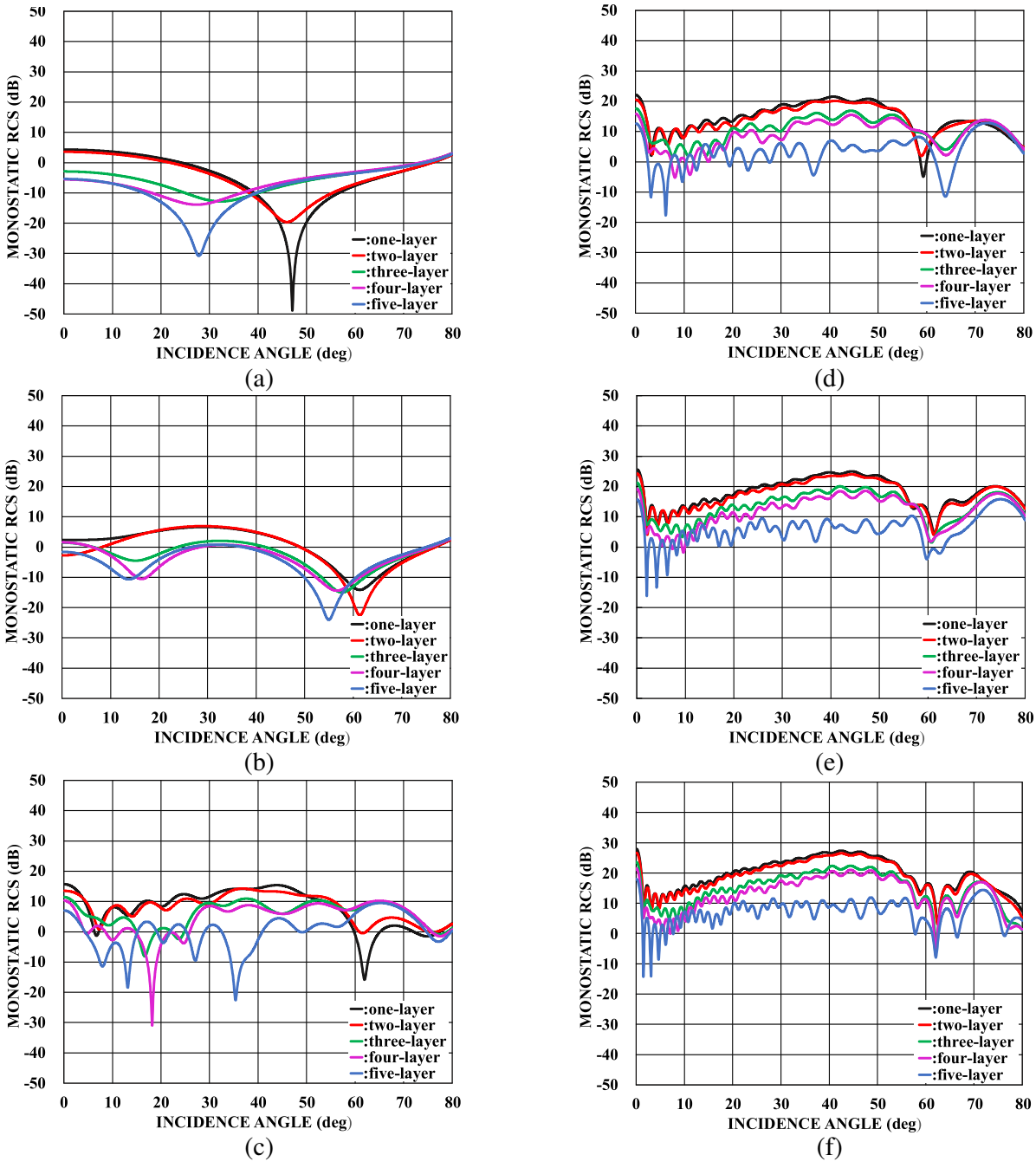

Figure 2. Monostatic RCS [dB] as a function of incidence angle θ_0 for $L_1/2b = 0.5$, $kt = 1.57$. (a) $kb = 1.57$. (b) $kb = 3.14$. (c) $kb = 15.7$. (d) $kb = 31.4$. (e) $kb = 47.1$. (f) $kb = 62.8$.

can be regarded as a single half-plane of zero thickness. In addition, the ratio $L_1/2b$ is as large as 5.0 in Fig. 5(a) (i.e., material-loaded regions are located far from the waveguide opening) and hence, the multilayer loading cannot be observed in the far field region. Comparing the RCS characteristics for the five curves (single- to five-layer material loading) in each figure significant RCS reduction is observed

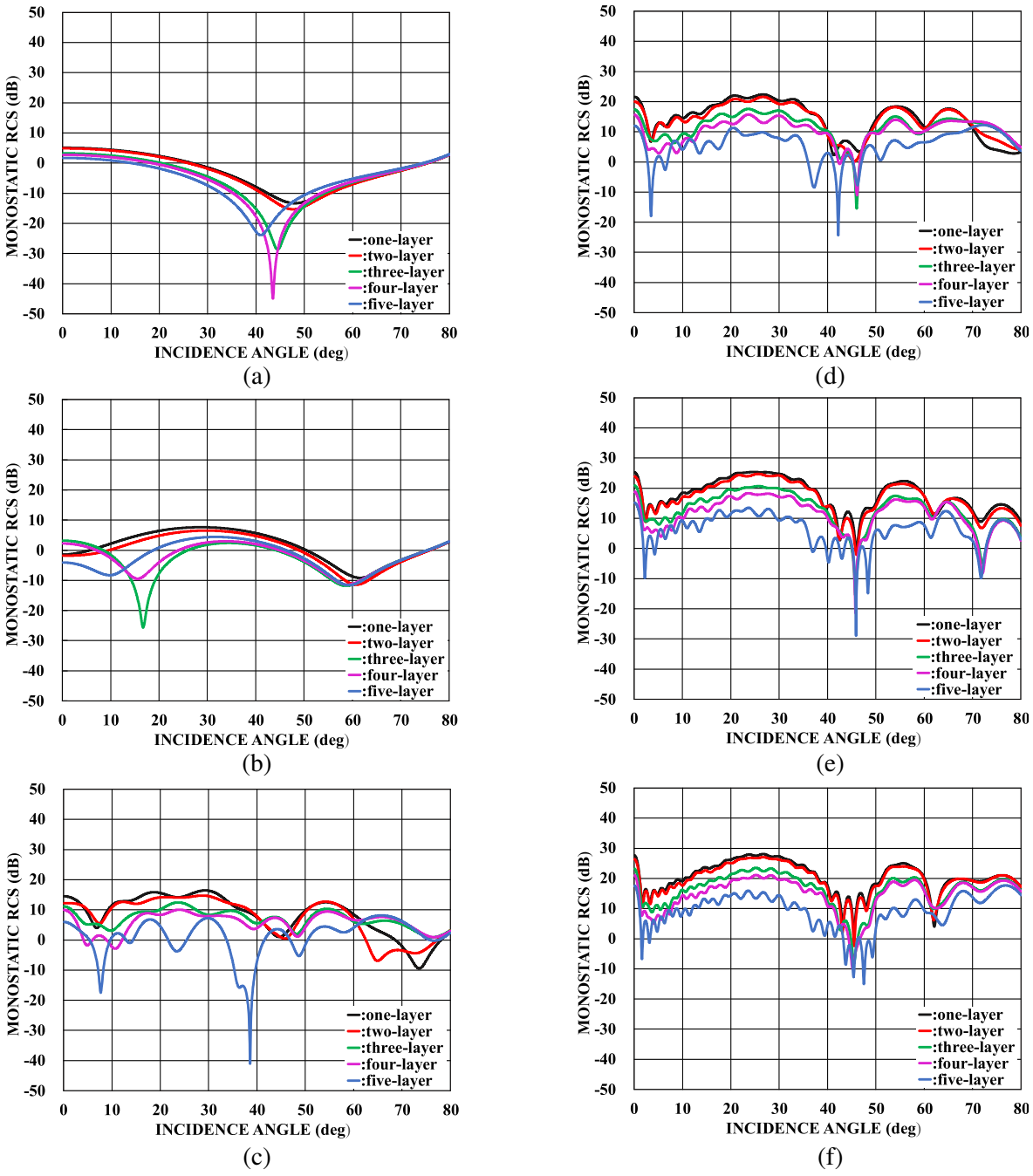

Figure 3. Monostatic RCS [dB] as a function of incidence angle θ_0 for $L_1/2b = 1.0$, $kt = 1.57$. Other particulars are the same as in Fig. 2. (a) $kb = 1.57$. (b) $kb = 3.14$. (c) $kb = 15.7$. (d) $kb = 31.4$. (e) $kb = 47.1$. (f) $kb = 62.8$.

at near-normal incidence ($\theta_0 = 0°$) for all figures except $kb = 1.57$. Therefore, it is inferred that for near normal incidence, the five-layer loading results in better RCS reduction over a wide frequency range. From these results, it can be confirmed that multilayer lossy materials can be used as broadband absorbing structures.

Next, we shall investigate frequency dependences of the RCS to make more thorough interpretation of the backscattering characteristics. Fig. 6 shows the normalized monostatic RCS as a function of normalized frequency kb for angles of incidence $\theta_0 = 0°$, $30°$, and $60°$, $L_1/2b = 1.0$. Five different

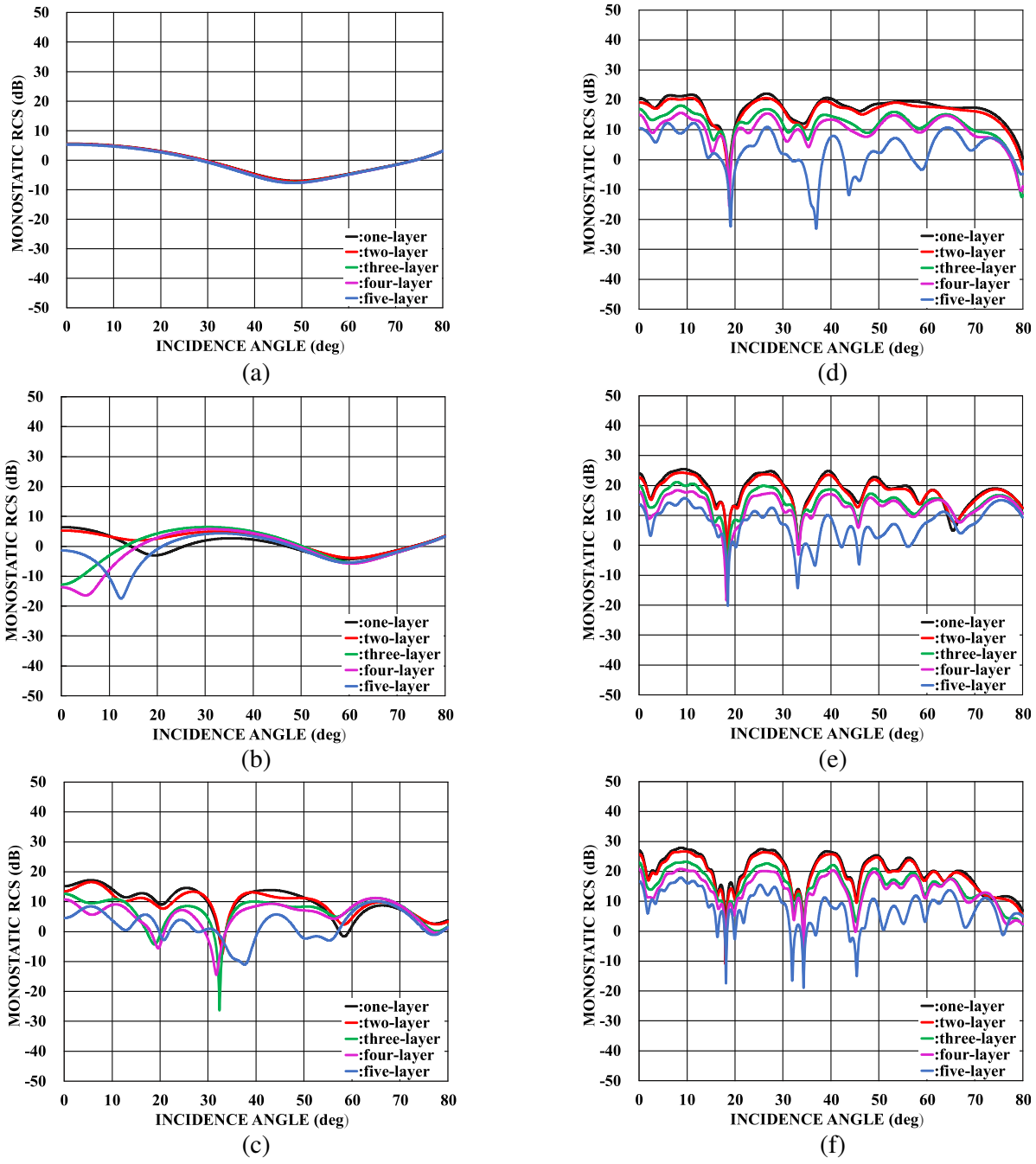

Figure 4. Monostatic RCS [dB] as a function of incidence angle θ_0 for $L_1/2b = 3.0$, $kt = 1.57$. Other particulars are the same as in Fig. 2. (a) $kb = 1.57$. (b) $kb = 3.14$. (c) $kb = 15.7$. (d) $kb = 31.4$. (e) $kb = 47.1$. (f) $kb = 62.8$.

geometries are again considered: waveguides with one-, two-, three-, four-, and five-layer material loading. The material properties and the layer thicknesses are the same as in Fig. 3. From Fig. 6, we can see that, for the single-layer loading, the average RCS level increases with an increase of kb, whereas for the multiple-layer loading, the RCS is reduced over the entire frequency range as shown in the figure. When comparing properties of the single- and multi-layer loadings, the RCS reduction in the five-layer case is significant. Therefore, this also demonstrates that multilayer lossy materials can be efficiently used as broadband absorbing structures. In the numerical example of Figs. 6(a), 6(b) and 6(c), we find

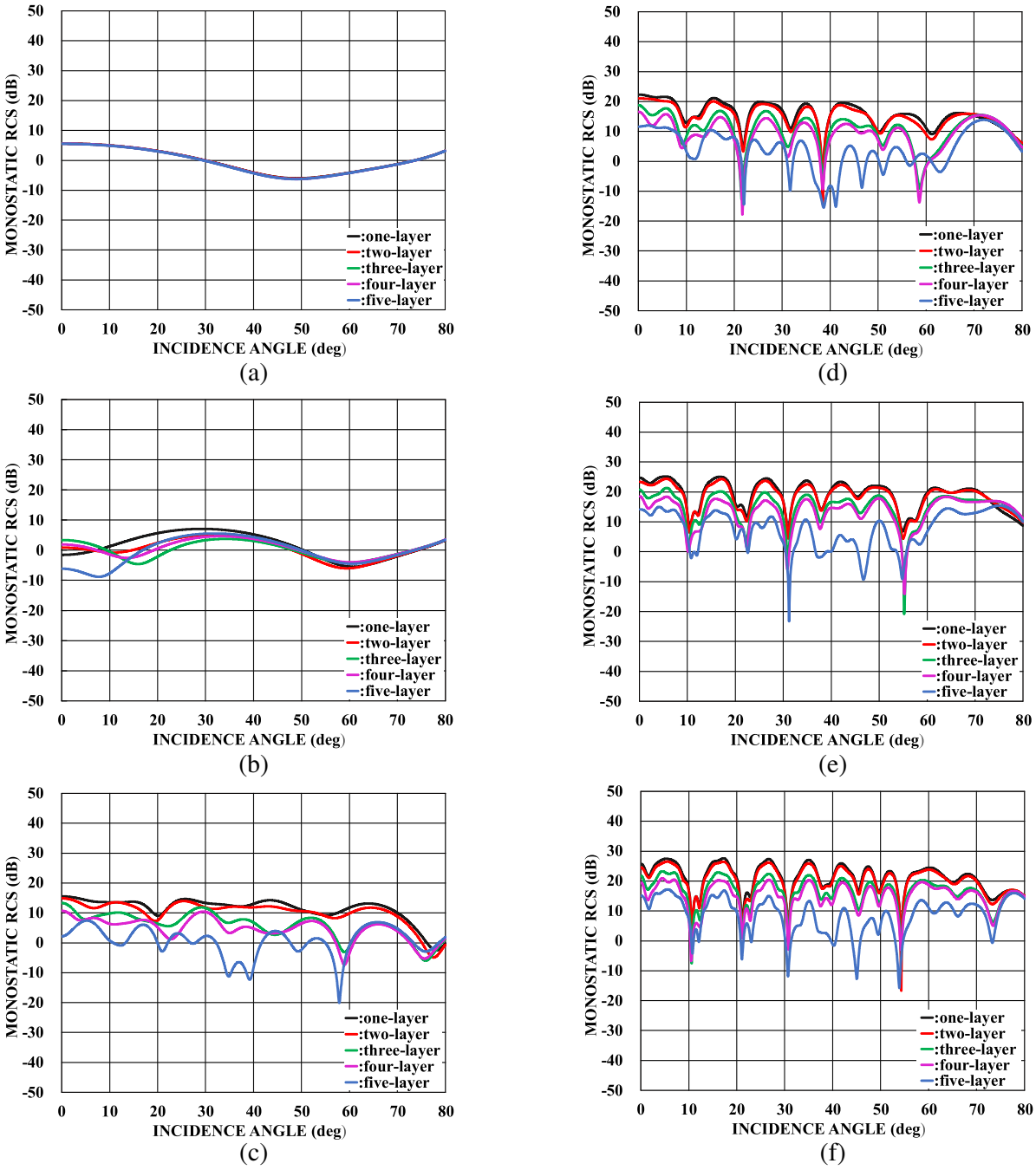

Figure 5. Monostatic RCS [dB] as a function of incidence angle θ_0 for $L_1/2b = 5.0$, $kt = 1.57$. Other particulars are the same as in Fig. 2. (a) $kb = 1.57$. (b) $kb = 3.14$. (c) $kb = 15.7$. (d) $kb = 31.4$. (e) $kb = 47.1$. (f) $kb = 62.8$.

that, with an increase of the incidence angle from $\theta_0 = 0°$ to 60°, the resonance phenomena are seen. In particular for the $\theta_0 = 0°$, waves incident on the material surface are simply reflected back, so that the RCS characteristics are of relatively smooth curves. However, as the incidence angle increases, the multiple reflection occurs inside the waveguide, which results in waveguide resonances.

The main purpose of this section is to investigate how the multi-layer lossy material loading inside the waveguide leads to better RCS reduction. The choice of optimal material parameters is important, but this is beyond the scope of this paper. This may be a future research direction for our research.

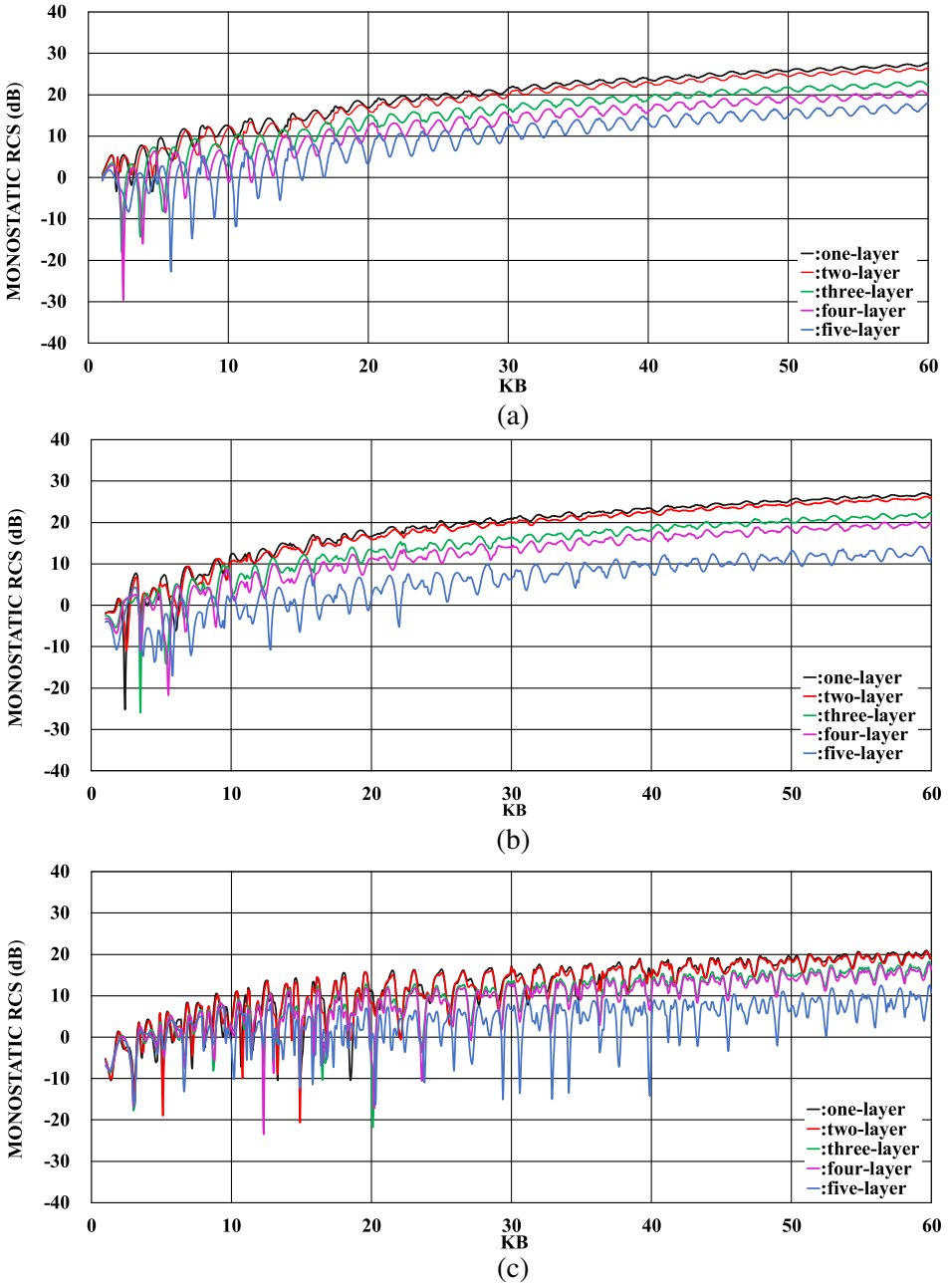

Figure 6. Monostatic RCS [dB] versus normalized frequency kb for $\theta_0 = 0°$, 30°, and 60°, $L_1/2b = 1.0$, $kt = 1.57$. Other particulars are the same as in Fig. 2. (a) $\theta_0 = 0°$. (b) $\theta_0 = 30°$. (c) $\theta_0 = 60°$.

9. CONCLUSION

In this paper, we have used the Wiener-Hopf technique to analyze the E-polarized plane wave diffraction rigorously by a semi-infinite parallel-plate waveguide with five-layer material loading. The result provides an important generalization of the problem treated in our previous paper [37]. It should be noted that the final solution obtained in this paper is uniformly valid for arbitrary waveguide dimension. We have presented representative numerical examples for various physical parameters, and discussed the backscattering characteristics of the waveguide in detail. The diffraction problem involving the same waveguide geometry for the H-polarized plane wave incidence is currently under investigation, and the results will be presented in a separate paper.

REFERENCES

1. Knott, E. F., J. Shaeffer, and M. Tuley, *Radar Cross Section*, 2nd Edition, SciTech, Raleigh, 2004.
2. Balanis, C. A., *Advanced Engineering Electromagnetics*, 2nd Edition, Wiley, New York, 2012.
3. Stone, W. R., Ed., *Radar Cross Sections of Complex Objects*, IEEE Press, New York, 1990.
4. Bhattacharyya, A. K. and D. L. Sengupta, *Radar Cross Section Analysis and Control*, Artech House, Boston, 1991.
5. Bernard, J. M. L., G. Pelosi, and P. Ya. Ufimtsev, "Special issue on radar cross section of complex objects," *Ann. Telecommun.*, Vol. 50, 1995.
6. Michielssen, E., J. M. Sajer, S. Ranjithan, and R. Mittra, "Design of lightweight, broad-band microwave absorbers using genetic algorithms," *IEEE Trans. Microwave. Theory Tech.*, Vol. 41, 1024–1031, 1993.
7. Zhou, D., X. Huang, and Z. Du, "Analysis and design of multilayered broadband radar absorbing metamaterial using the 3-D printing technology-based method," *IEEE Antennas Wireless Propag. Lett.*, Vol. 16, 133–136, 2017.
8. Toktas, A., D. Ustun, and M. Tekbas, "Multi-objective design of multilayer radar absorber using surrogate-based optimization," *IEEE Trans. Microwave. Theory Techn.*, Vol. 67, 3318–3329, 2019.
9. Pathak, P. H. and R. J. Bukholder, *Electromagnetic Radiation, Scattering, and Diffraction*, Wiley, New York, 2021.
10. Lee, C. S. and S.-W. Lee, "RCS of a coated circular waveguide terminated by a perfect conductor," *IEEE Trans. Antennas Propagat.*, Vol. 35, 391–398, 1987.
11. Altintas, A., P. H. Pathak, and M. C. Liang, "A selective modal scheme for the analysis of EM coupling into or radiation from large open-ended waveguides," *IEEE Trans. Antennas Propagat.*, Vol. 36, 84–96, 1988.
12. Ling, H., R.-C. Chou, and S.-W. Lee, "Shooting and bouncing rays: Calculating the RCS of an arbitrary shaped cavity," *IEEE Trans. Antennas Propagat.*, Vol. 37, 194–205, 1989.
13. Pathak, P. H. and R. J. Burkholder, "Modal, ray, and beam techniques for analyzing the EM scattering by open-ended waveguide cavities," *IEEE Trans. Antennas Propagat.*, Vol. 37, 635–647, 1989.
14. Pathak, P. H. and R. J. Burkholder, "A reciprocity formulation for the EM scattering by an obstacle within a large open cavity," *IEEE Trans. Microwave Theory Tech.*, Vol. 41, 702–707, 1993.
15. Lee, R. and T.-T. Chia, "Analysis of electromagnetic scattering from a cavity with a complex termination by means of a hybrid ray-FDTD method," *IEEE Trans. Antennas Propagat.*, Vol. 41, 1560–1569, 1993.
16. Ohnuki, S. and T. Hinata, "Radar cross section of an open-ended rectangular cylinder with an iris inside the cavity," *IEICE Trans. Electron.*, Vol. E81-C, 1875–1880, 1998.
17. Kim, D. Y., H. Lim, J. H. Han, W. Y. Song, and N. H. Myung, "RCS reduction of open-ended circular waveguide cavity with corrugations using mode matching and scattering matrix analysis," *Progress In Electromagnetics Research*, Vol. 146, 57–69, 2014.
18. Xiang, S., G. Xiao, and J. Mao, "A generalized transition matrix model for open-ended cavity with complex internal structures," *IEEE Trans. Antennas Propagat.*, Vol. 64, 3920–3930, 2016.
19. Zhou, Y., Y. Yan, J. Xie, H. Chen, G. Zhang, F. Li, L. Zhang, X. Wang, X. Weng, P. Zhou, et al., "Broadband RCS reduction for electrically-large open-ended cavity using random coding metasurfaces," *Journal of Physics D: Applied Physics*, Vol. 52, 315303, 2019.
20. Serizawa, H. and K. Hongo, "Radiation from a flanged rectangular waveguide," *IEEE Trans. Antennas Propagat.*, Vol. 53, 3953–3962, 2005.
21. Sato, R. and H. Shirai, "Electromagnetic plane wave scattering by a loaded trough on a ground plane," *IEICE Trans. Electron.*, Vol. E77-C, 1983–1989, 1994.
22. Büyükaksoy, A., F. Birbir, and E. Erdogan, "Scattering characteristics of a rectangular groove in a reactive surface," *IEEE Trans. Antennas and Propagat.*, Vol. 43, 1450–1458, 1995.

23. Cetiner, B. A., A. Büyükaksoy, and F. Güneş, "Diffraction of electromagnetic waves by an openended parallel plate waveguide cavity with impedance walls," *Progress In Electromagnetics Research*, Vol. 26, 165–197, 2000.
24. Noble, B., *Methods Based on the Wiener-Hopf Technique for the Solution of Partial Differential Equations*, Pergamon, London, 1958.
25. Mittra, R. and S.-W. Lee, *Analytical Techniques in the Theory of Guided Waves*, Macmillan, New York, 1971.
26. Kobayashi, K., "Wiener-Hopf and modified residue calculus techniques," *Analysis Methods for Electromagnetic Wave Problems*, E. Yamashita (ed.), Chap. 8, Artech House, Boston, 1990.
27. Daniele, V. G. and G. Lombardi, *Scattering and Diffraction by Wedges 1, The Wiener-Hopf Solution-theory*, Wiley-ISTE, Hoboken, 2020.
28. Daniele, V. G. and G. Lombardi, *Scattering and Diffraction by Wedges 2, The Wiener-Hopf Solution-advanced Applications*, Wiley-ISTE, Hoboken, 2020.
29. Kobayashi, K. and A. Sawai, "Plane wave diffraction by an openended parallel plate waveguide cavity," *Journal of Electromagnetic Waves and Applications*, Vol. 6, 475–512, 1992.
30. Kobayashi, K., S. Koshikawa, and A. Sawai, "Diffraction by a parallel-plate waveguide cavity with dielectric/ferrite loading: part I — the case of E polarization," *Progress In Electromagnetics Research*, Vol. 8, 377–426, 1994.
31. Koshikawa, S. and K. Kobayashi, "Diffraction by a parallel-plate waveguide cavity with dielectric/ferrite loading: part II — the case of H polarization," *Progress In Electromagnetics Research*, Vol. 8, 427–458, 1994.
32. Zheng, J. P. and K. Kobayashi, "Plane wave diffraction by a finite parallel-plate waveguide with four-layer material loading: part I — the case of E polarization," *Progress In Electromagnetics Research B*, Vol. 6, 1–36, 2008.
33. Shang, E. H. and K. Kobayashi, "Plane wave diffraction by a finite parallel-plate waveguide with four-layer material loading: part II — the case of H polarization," *Progress In Electromagnetics Research B*, Vol. 6, 267–294, 2008.
34. Koshikawa, S., D. Colak, A. Altintas, K. Kobayashi, and A. I. Nosich, "A comparative study of RCS predictions of canonical rectangular and circular cavities with double-layer material loading," *IEICE Trans. Electron.*, Vol. E80-C, 1457–1466, 1997.
35. Koshikawa, S. and K. Kobayashi, "Diffraction by a terminated, semi-infinite parallel-plate waveguide with three-layer material loading," *IEEE Trans. Antennas and Propagat.*, Vol. 45, 949–959, 1997.
36. Koshikawa, S. and K. Kobayashi, "Diffraction by a terminated, semi-infinite parallel-plate waveguide with three-layer material loading: the case of H polarization," *Electromagnetic Waves & Electronic Systems*, Vol. 5, 13–23, 2000.
37. Shang, E. H. and K. Kobayashi, "Diffraction by a terminated, semi-infinite parallel-plate waveguide with four-layer material loading", *Progress In Electromagnetics Research B*, Vol. 12, 139–162, 2009.
38. Meixner, J., "The behavior of electromagnetic field at edges," *IEEE Trans. Antennas and Propagat.*, Vol. 20, 442–446, 1972.